Wind–Evaporation Feedback and Abrupt Seasonal Transitions of Weak, Axisymmetric Hadley Circulations

WILLIAM R. BOOS AND KERRY A. EMANUEL

Program in Atmospheres, Oceans and Climate, Massachusetts Institute of Technology, Cambridge, Massachusetts

(Manuscript received 31 August 2007, in final form 7 December 2007)

ABSTRACT

For an imposed thermal forcing localized off the equator, it is known that conservation of absolute angular momentum in axisymmetric flow produces a nonlinear response once the forcing exceeds a critical amplitude. It is shown here that, for a moist atmosphere in convective quasi-equilibrium, the combination of wind-dependent ocean surface enthalpy fluxes and zonal momentum advection can provide a separate feedback that causes the meridional flow to evolve nonlinearly as a function of a sea surface temperature (SST) forcing, even if an angular momentum–conserving response is not achieved. This wind–evaporation feedback is examined in both an axisymmetric primitive equation model and a simple model that retains only a barotropic and single baroclinic mode. Only SST forcings that do not produce an angular momentum–conserving response are examined here. The wind–evaporation feedback is found to be inhibited in models with linear dynamics because the barotropic component of the Hadley circulation, which is coupled to the baroclinic circulation via surface drag, keeps surface winds small compared to upper-level winds. In models with nonlinear dynamics, the convergence of zonal momentum into the ascending branch of the cross-equatorial Hadley cell can create barotropic westerlies that constructively add to the baroclinic wind at the surface, thereby eliminating the inhibition of the wind–evaporation feedback. The possible relevance of these results to the onset of monsoons is discussed.

1. Introduction

Steady-state, axisymmetric solutions for the circulation in a differentially heated fluid on a rotating sphere have been advanced over the past few decades as a means of understanding the Hadley circulation (e.g., Schneider 1977; Held and Hou 1980). The associated theory emphasizes conservation of absolute angular momentum in the free troposphere, which results in a nonlinear dependence of circulation strength and extent on the imposed thermal forcing.

Results of this theory have been used to explain certain aspects of the seasonal cycle of the Hadley circulation. Lindzen and Hou (1988) showed that the steady, axisymmetric response to a heating with a peak displaced just a few degrees off the equator exhibits a strong asymmetry in the strength and meridional extent of the summer and winter Hadley cells, consistent with observations. Plumb and Hou (1992, hereafter PH92) showed that the strength of steady, axisymmetric meridional flow increases nonlinearly as the magnitude of a thermal forcing localized off the equator is enhanced beyond a threshold value. They suggested that this threshold behavior might be relevant to the seasonal onset of monsoons, but noted that the roles of time dependence and zonal asymmetries need to be assessed.

The effect of time dependence on axisymmetric theory has only begun to be explored. Fang and Tung (1999) examined a version of the axisymmetric dry model used by Lindzen and Hou (1988), but with a time-dependent forcing. They found that there was no abrupt change in the circulation as the maximum of the thermal forcing was moved meridionally in a seasonal cycle, primarily because the circulation did not achieve equilibrium with its forcing during the course of this seasonal cycle. The dry axisymmetric models used by Fang and Tung (1999) and PH92 equilibrate on time scales on the order of 100 days, which is longer than the time scale associated with the seasonal cycle of earth's

Corresponding author address: William R. Boos, Massachusetts Institute of Technology, Rm 54-1721, 77 Massachusetts Ave., Cambridge, MA 02139.
E-mail: billboos@alum.mit.edu

DOI: 10.1175/2007JAS2608.1

insolation forcing.[1] However, moist axisymmetric models with stratifications and rates of radiative cooling similar to those of the earth's tropics will equilibrate much faster, an issue we discuss in an appendix and illustrate in the body of this paper. Therefore, it is not reasonable to apply a time-varying forcing having a 365-day period to a model with an equilibration time scale on the order of 100 days and expect the results to be relevant to the seasonal cycle of earth's Hadley circulation.

The fact that moist axisymmetric models equilibrate on a time scale shorter than that of the earth's seasonal cycle is illustrated by the results of Zheng (1998), who extended the study of PH92 using a moist axisymmetric model forced by an off-equatorial sea surface temperature (SST) anomaly. Zheng (1998) confirmed that the circulation entered an angular momentum–conserving (AMC) regime once the magnitude of the SST anomaly exceeded a certain threshold, and found that an abrupt, nonlinear onset of the summer circulation occurred when the SST forcing was varied in a seasonal cycle. It is of interest that Zheng (1998) did not use wind-dependent surface enthalpy fluxes in his model runs, because Numaguti (1995) found that wind-dependent ocean evaporation was needed to obtain an abrupt poleward shift in the peak precipitation as a prescribed SST maximum was gradually shifted poleward in a three-dimensional general circulation model (GCM). Based on the diagnostics presented by Numaguti (1995), it is difficult to judge whether the meridional flow in his model increased nonlinearly as a function of the forcing. The forcing used by Numaguti (1995) was also not localized off the equator, and so is a better analog of that used by Lindzen and Hou (1988) than that used by PH92.

Although this paper only explores axisymmetric dynamics, zonally asymmetric eddies may play an important role in Hadley circulation dynamics. For thermal forcings centered on the equator in a three-dimensional model with zonally symmetric boundary conditions, Walker and Schneider (2006) found that the strength of the Hadley circulation was directly related to the eddy momentum flux divergence, and that scalings based on the assumptions of axisymmetric angular momentum conservation did not hold. However, when the peak thermal forcing was displaced sufficiently far from the equator, their model produced cross-equatorial flow that nearly conserved absolute angular momentum, at least in its free-tropospheric ascending branch. Schneider and Bordoni (2008) found that abrupt transitions between the eddy-controlled equinoctial regime and the AMC solsticial regime occurred in a model with a seasonally varying forcing, and discussed the similarity between the dynamics of this transition and the onset and end of monsoons. While eddy transports may thus play an important role in seasonal Hadley dynamics, we shall demonstrate that a wind–evaporation feedback may also play an important role, and that this feedback is sufficiently complex to merit initial examination in idealized two-dimensional models.

The desire to explain the seasonal evolution of monsoons motivates this and many previous works on abrupt seasonal transitions. Several regional summer monsoons do begin abruptly, by which we mean they evolve faster than can be explained by a linear response to their forcing. The start of precipitation and the reversal of zonal wind which mark the beginning of the South Asian and Australian summer monsoons occur on time scales shorter than those contained in the insolation forcing (Murakami et al. 1986; Wheeler and McBride 2005; Webster et al. 1998). Mapes et al. (2005) found that even when the period of the solar and SST forcings was increased by a factor of 5 in an atmospheric GCM, the onset of summer precipitation over India still seemed to occur over the same one- to two-week time scale as in a control run.

In this paper, we use results from axisymmetric models to show how wind–evaporation feedback might produce such an abrupt seasonal transition. Although it may be difficult to say how an idealized model of the global Hadley circulation relates to the various regional monsoons, the fact that more than half of the global low-level cross-equatorial mass flux occurs in the Somali jet (e.g., Findlater 1969) would seem to ensure that the South Asian monsoon, at least, projects strongly onto the zonal mean Hadley circulation during boreal summer. Wind speeds in the off-equatorial, southwesterly part of the Somali jet do intensify abruptly near the start of the Indian monsoon (Krishnamurti et al. 1981; Halpern and Woiceshyn 1999). Nevertheless, further work is needed to reconcile this fact with the finding that a scalar index of the climatological, monthly-mean Hadley circulation projects almost entirely onto a sinusoid with a period of 365 days (Dima and Wallace 2003). Prive and Plumb (2007) examined the applicability of nonlinear axisymmetric theories for the Hadley circulation to steady-state monsoons, and found that zonal asymmetries in the land surface could cause profound changes in the circulation that could not be described by axisymmetric frameworks. A similar study of the process of monsoon onset has yet to be performed, and we see the present paper as a first step in a process

[1] A sinusoid with a period of 365 days varies with a time scale $\tau = 58$ days, if τ is interpreted as the e-folding time.

which might later employ more complex spatial domains representative of real-world monsoons.

The main goal of this paper is to examine the effect of wind-induced surface heat exchange (WISHE) on the seasonal cycle of meridional flow in the context of previous studies of nonlinear axisymmetric theory. In particular, we use axisymmetric (non-eddy-resolving) models forced by thermal maxima localized off the equator, as in PH92. One of our main results will be that WISHE can produce an abrupt, nonlinear intensification of meridional flow as a function of such a forcing, by a mechanism distinct from that of a transition to an AMC regime. In examining this effect of WISHE, we will limit our focus to weak SST forcings that do not produce an AMC circulation. The effect of WISHE for stronger forcings that do produce AMC flow is not trivial and will be explored in a separate paper.

The next section of this paper begins by presenting results from a dry primitive equation model to emphasize that meridional flow generated by a near-linear viscous response can be just as strong as that occurring in a nonlinear AMC regime; any feedback between the thermal forcing and the circulation could thus produce a rapid change in the circulation without involving nonlinear dynamics. A moist primitive equation model is then used to show that a wind–evaporation feedback can produce a circulation that depends nonlinearly on the SST forcing, but that this feedback requires the nonlinear advection of zonal momentum even though the free-tropospheric circulation is not in an AMC regime. An idealized two-mode model of tropospheric flow is introduced to explain this interaction between wind–evaporation feedback and zonal momentum advection. We conclude by discussing the relevance of these results to monsoons and some possible effects of processes omitted from these idealized models. An appendix presents a scale estimate for the equilibration time of both dry and moist axisymmetric models.

2. Primitive equation model

The time-dependent behavior of Hadley circulations is examined in both dry and moist versions of the axisymmetric (latitude–height) GCM used by Pauluis and Emanuel (2004) and Pauluis (2004). The model dynamics are based on the Massachusetts Institute of Technology (MIT) GCM (Marshall et al. 1997; Adcroft et al. 1999; Marshall et al. 2004), but a series of alternate parameterizations is used for subgrid-scale physics. The model domain is a partial sphere extending between rigid walls at 64°N and 64°S, with 1° meridional resolution on a staggered spherical polar grid. There are 40 pressure levels with 25-hPa resolution, from 1000 hPa to a rigid lid at 0 hPa, and no representation of orography. Viscosity is represented by the vertical diffusion of momentum with a coefficient of 100 $\mathrm{Pa}^2\ \mathrm{s}^{-1}$. Frictional stresses in the planetary boundary layer are represented by vertically homogenizing horizontal velocities in the lowest 200 hPa of the atmosphere over a time scale of 20 min, and a bulk flux formula for momentum is used to represent surface drag. An eighth-order Shapiro filter is used to reduce small-scale horizontal noise in the temperature, specific humidity, and horizontal wind fields.

Instead of diagnosing the spatial extremum of the overturning streamfunction as a metric for circulation intensity, we use the meridional flow integrated both vertically through the boundary layer (800–1000 hPa) and meridionally over all model latitudes, a quantity hereafter called the PBL flow. The PBL flow has the advantage of being a single scalar that is continuously relevant during the transition from summer to winter, whereas one must alternately choose the maximum and minimum streamfunction to represent changes in the seasonal strength of the Hadley circulation. This becomes relevant when the thermal forcing is prescribed to vary in a seasonal cycle. Because the PBL flow involves a meridional integral, it does not measure the equatorially antisymmetric component of the streamfunction. We chose a dynamical boundary layer depth of 200 hPa in order to constrain most of the meridional mass flux in the lower branch of the Hadley circulation to move through this boundary layer, as Pauluis (2004) showed that shallower PBL depths in an axisymmetric model resulted in a larger fraction of the low-level flow crossing the equator in the free troposphere.

a. Dry model

1) Dry model configuration

In a dry version of the axisymmetric MIT GCM, the circulation is forced by relaxation of temperature over a spatially uniform time scale of 10 days to a prescribed distribution T_{eq} similar to that used by PH92:

$$T_{\mathrm{eq}} = T_0 + T_{\mathrm{max}} \frac{\pi}{2} \sin\left(\pi \frac{p_0 - p}{p_0}\right) \cos^2\left(\frac{\pi}{2} \frac{\phi - \phi_0}{\Delta\phi}\right). \tag{1}$$

This is used to specify T_{eq} only between $\phi_0 + \Delta\phi$ and $\phi_0 - \Delta\phi$; outside this range T_{eq} is set to T_0. Here p_0 is pressure at the lowest model level, $\phi_0 = 25°\mathrm{N}$, and $\Delta\phi = 15°$. This gives an equilibrium temperature with no meridional gradient outside the range 10°–40°N and an extremum centered at 25°N and 500 hPa.

Most integrations of the dry model use an isothermal

background state with $T_0 = 200$ K. As discussed in the appendix, use of an isothermal background state will produce relatively weak meridional velocities and thus an equilibration time scale for absolute angular momentum M of about 165 days, which is much longer than the time scale of earth's seasonal insolation forcing. This long time scale is purposely chosen in order to provide a clear separation in time between the equilibrated, AMC state and an initial transient state in which the atmospheric dynamics are predominantly linear. Furthermore, this long equilibration time scale is similar to that used by PH92 and Fang and Tung (1999), and so allows results presented herein to be more easily compared with their findings. A model integration is also performed using a background state having near-neutral stratification, with $\partial_z T_0 = 0.9g/c_p$, which reduces the time scale for M advection to about 15 days. The moist model, discussed below, also equilibrates on a time scale shorter than that of the forcing.

We examine the equilibrated response to steady forcings as well as the time-dependent response to a seasonally varying forcing. In all cases, the initial model state used was that of an atmosphere at rest with meridionally uniform temperature T_0. To avoid high-amplitude initial transients, the off-equatorial anomaly of equilibrium temperature was increased from zero for the steady forcings according to

$$T_{\max} = \theta_m(1 - e^{-t/\tau_i}), \tag{2}$$

with $\tau_i = 30$ days. Three separate integrations with steady forcings were performed, using $\theta_m = 5$, 10, and 15 K. For the seasonal forcing, $T_{\max}$ in (1) was varied according to

$$T_{\max} = \theta_m \cos\left(2\pi \frac{t}{365 \text{ days}}\right), \tag{3}$$

where t is time in days and $\theta_m = 15$ K.

2) DRY MODEL RESULTS

As in PH92, the response to steady forcings took hundreds of days to achieve a steady state, at which time the equilibrated PBL flow depended nonlinearly on θ_m (Fig. 1). The streamfunction maximum (not shown) behaved similarly to the PBL flow, although it achieved a steady state more quickly and did not have an initial transient peak for $\theta_m = 15$ K. The existence of the initial peak in PBL flow around day 80 for all values of θ_m more clearly divides the evolution of the flow into two regimes: an initial transient phase where the PBL flow scales nearly linearly with θ_m, and a steady state where the PBL flow depends nonlinearly on θ_m. The small kink at day 400 in the PBL flow for $\theta_m = 15$ K is associated with inertial instabilities that produce roll circulations of high vertical wavenumber (Dunkerton 1989 discusses this behavior in more detail). These inertial rolls are symptomatic of the fact that this value of θ_m was near the maximum for which numerically stable solutions could be achieved.

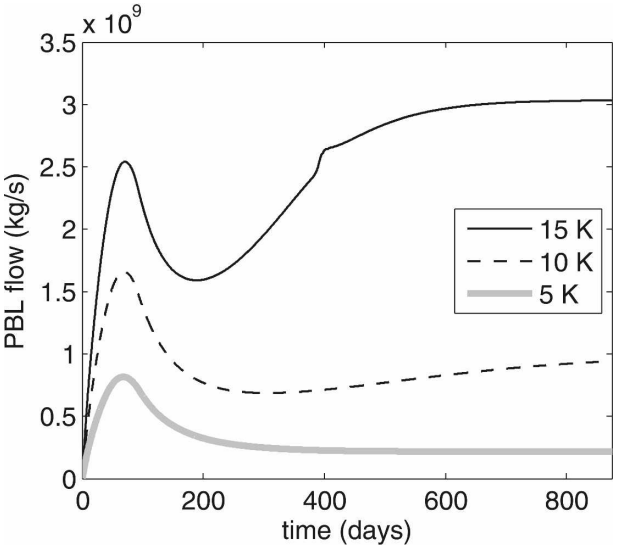

FIG. 1. Time evolution of the PBL flow (defined as the meridional wind integrated vertically and meridionally in the boundary layer) for the dry GCM with steady forcing. The three curves correspond to forcings with different values of θ_m, which sets the magnitude of the off-equatorial equilibrium temperature anomaly.

The model evolution can be understood in terms of the evolution of M. During the first 100 days of integration for $\theta_m = 15$ K, the M distribution is only slightly perturbed from its initial state of solid-body rotation, although the streamfunction and PBL flow reach amplitudes nearly as large as in equilibrium (Fig. 2, left panel). After equilibration, which takes more than 500 days, the M field has undergone considerable homogenization in the upper troposphere with the zero contour of absolute vorticity displaced to about 20°S (Fig. 2, right panel). During both the initial transient peak and the final steady state, most of the lower branch of the meridional circulation flows through the boundary layer, peak ascent occurs slightly equatorward of ϕ_0, and a weak summer cell exists in the midlatitude summer hemisphere, all of which are consistent with the axisymmetric results of Lindzen and Hou (1988) and Fang and Tung (1999). The streamfunction maximum is fairly low in the free troposphere, suggesting that these results are free of any amplification of the circulation due to the rigid-lid upper-boundary condition (Walker and Schneider 2005).

The time evolution thus seems to be a superposition

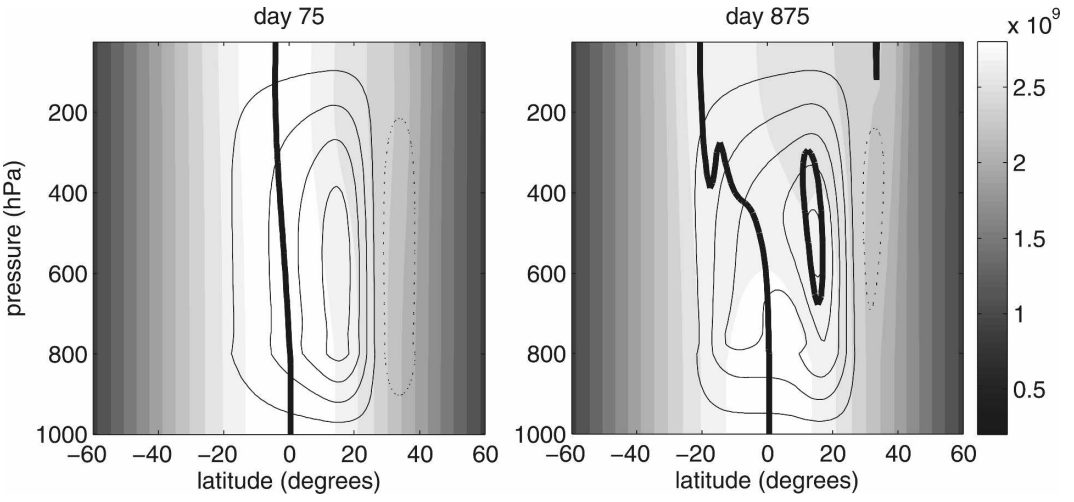

FIG. 2. Absolute angular momentum (shading) and meridional streamfunction (thin contours) for the dry GCM with steady forcing and $\theta_m = 15$ K (left) at the initial transient peak and (right) after the model achieved a steady state. Thick solid line is the zero absolute vorticity contour. Streamfunction contour interval is 1×10^{10} kg s^{-1}, starting at 0.5×10^{10} kg s^{-1}, with negative contours (denoting clockwise rotation) dashed. Angular momentum contour interval is 0.2×10^9 m^2 s^{-1}.

of a relatively rapid and linear thermally dominated adjustment followed by a slow, nonlinear adjustment dominated by M advection. Although this in many ways restates some results of PH92, we include this discussion to emphasize a particular point: changes in the thermal forcing can produce a linear response in the strength of the circulation within a few inertial periods (the initial transient peak occurs after 80 days because of the spinup used for the forcing). If the thermal forcing is not externally specified but depends on the circulation itself, feedbacks could occur because of interactions between the circulation and the forcing. Later sections of this paper will examine the particular case of a wind–evaporation feedback, but coupling between the circulation and the thermal forcing could also occur via radiation or other processes. Depending on the nature of these interactions, such feedbacks could operate in a regime where the atmospheric dynamics are predominantly linear and M advection is not important.

For the seasonally varying forcing, the circulation took less than 100 days to achieve a regular periodic cycle (not shown). After this initial adjustment time, the streamfunction and PBL flow peaked each year shortly before T_{eq} reached its maximum. We will refer to this time of peak PBL flow as the summer solstice, using the convention of boreal summer for $T_{\max} > 0$. The streamfunction and M distribution at this summer solstice, shown in Fig. 3, closely resemble those seen during the initial transient peak of the runs with steady forcing, without the folding over of M surfaces seen in the equilibrated response to the steady forcing. Contours of M tilt very slightly against the flow in the upper troposphere of the winter hemisphere, suggestive of their deformation by flow during the previous solstice. Also, the meridional width of the M peak near the equator is slightly larger for the seasonally varying forcing than for the steady forcing, suggesting that some homogenization is accomplished by the seasonally reversing meridional winds.

The PBL flow exhibits no abrupt transitions over time, although a slight nonlinearity is apparent between summer and winter seasons when the PBL flow is plot-

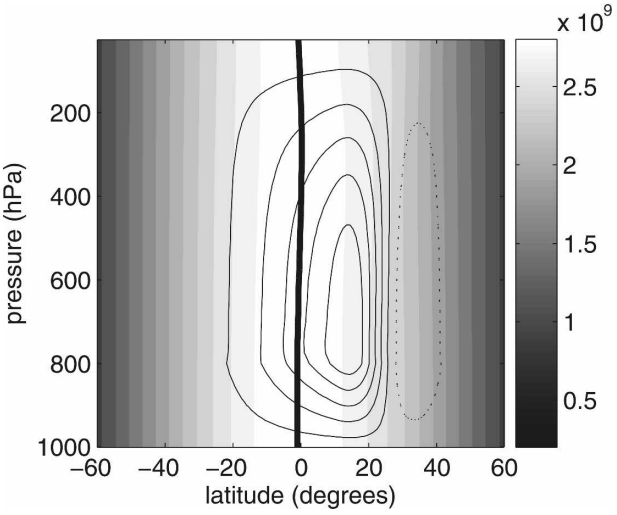

FIG. 3. As in Fig. 2, but for the dry GCM with seasonally varying forcing, at the time of largest PBL flow.

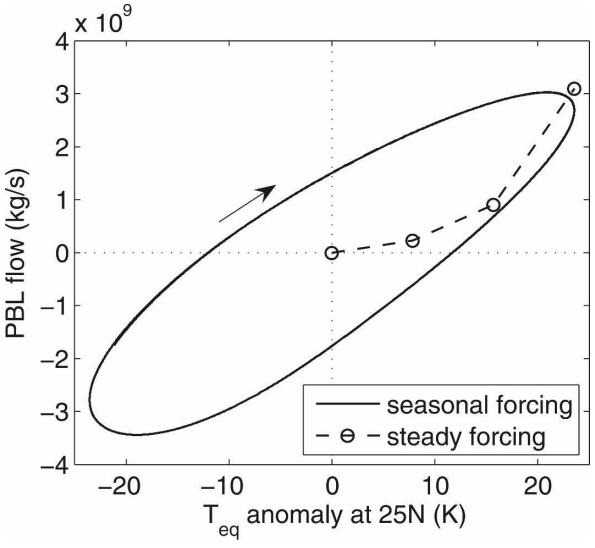

FIG. 4. Phase diagram of the PBL flow and the spatial extremum of the equilibrium temperature anomaly for the dry GCM. Solid line is for the run with seasonally varying forcing, with time progressing in the direction of the arrow. The circles connected by the dashed line denote the equilibrated response to steady forcings.

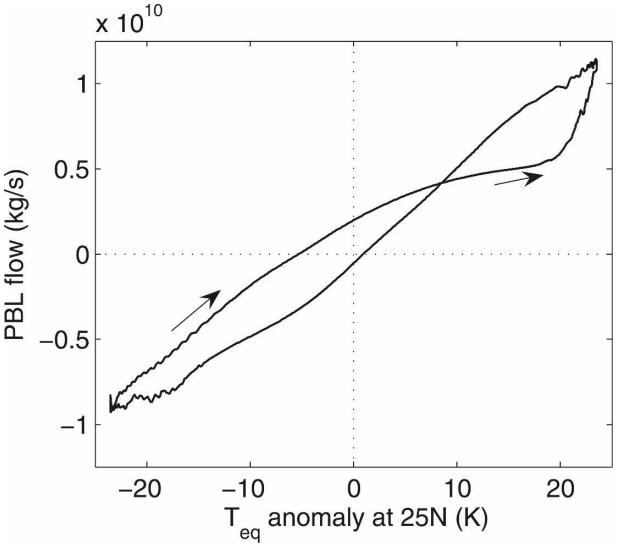

FIG. 5. As in Fig. 4, but the phase diagram for the dry GCM with a reduced background stratification ($\partial T_0/\partial z = 0.9\,\Gamma_d$) and a strong forcing ($\theta_m = 15$ K).

ted against the quantity $T_{\max}\pi/2$, which is the equilibrium temperature anomaly at 25°N (Fig. 4). This phase-space trajectory would be a perfect ellipse if the PBL flow varied linearly with $T_{\max}$ with only a phase lag between the two quantities. The equilibrated PBL flow for the steady forcings, also plotted on this phase diagram, increases nonlinearly with $T_{\max}$.

The PBL flow in the seasonally forced run leads $T_{\max}$, as shown by the clockwise phase-space trajectory. It is straightforward to show that this phase relationship is expected when the thermal relaxation time is short compared to the forcing period. If $T_{\max} = \sin(At)$ and T is assumed to lag $T_{\max}$ by Δt but to have the same frequency A, then a trigonometric identity can be used to write the Newtonian cooling as

$$Q = \frac{T_{\max} - T}{\tau} = \frac{2}{\tau}\cos\left(At - \frac{A\Delta t}{2}\right)\sin\frac{A\Delta t}{2}. \quad (4)$$

This shows that Q will lead $T_{\max}$ by $(\pi/2 - A\Delta t/2)$, which is slightly less than one-quarter cycle if Δt is much smaller than the forcing period. Linear theory for a sea breeze (Rotunno 1983), although formulated on an f plane instead of a sphere, predicts that the circulation will be in phase with Q so long as f is larger than the frequency of the thermal forcing, which is true for a forcing period of 365 days everywhere except within a tenth of a degree of the equator. Since M advection seems to be of minor importance for the evolution of the streamfunction for the seasonally varying forcing, the dynamics might be decently described by this linear theory, with Q in phase with the PBL flow and both leading $T_{\max}$ by one-quarter cycle. However, the PBL flow and $T_{\max}$ peak at nearly the same time, giving the major axis of the phase-space ellipse its positive slope and indicating that part of the circulation must be in phase with $T_{\max}$. So it would seem that the phase lag between $T_{\max}$ and the PBL flow explains why the phase trajectory is an ellipse rather than a straight line, but that a significant part of the flow is also in phase with $T_{\max}$. Similar phase relationships were obtained for an increased Newtonian cooling time scale of 30 days, as well as for a reduced viscosity of 10 $\text{Pa}^2\ \text{s}^{-1}$. This reduced viscosity was near the lowest value for which numerically stable solutions could be obtained. Integrations using smaller values of ϕ_0 and θ_m also produced circulations that evolved nearly linearly with $T_{\max}$.

If the time scale of M advection is smaller than that of variations in $T_{\max}$, then we expect the time evolution of a seasonally forced model to become nonlinear. This hypothesis is tested by using the reduced background stratification of $\partial_z T_0 = 0.9g/c_p$, for which M advection has an estimated time scale of around 15 days (see the appendix). When this model is integrated using the same value of $\theta_m = 15$ K in (3), the phase diagram shows that the sensitivity of the PBL flow to $T_{\max}$ does increase suddenly shortly before the summer solstice (Fig. 5). This trajectory deviates considerably from the ellipse expected for a linear response, and loosely resembles the figure "8" expected for two time series

where one evolves at twice the frequency of the other. At the time when the sensitivity of the PBL flow to $T_{\max}$ increases abruptly, the absolute vorticity near the model tropopause approached zero throughout much of the tropics (not shown), indicating that the abrupt transition is associated with the onset of M-conserving flow at upper levels. While a more comprehensive investigation would estimate model equilibration times as a function of the ratio of $\partial_z T_0$ to the Newtonian cooling rate, only these limiting cases are presented here for brevity.

b. Moist model

1) MOIST MODEL CONFIGURATION

In a moist version of the model, the circulation is forced by parameterized radiative cooling together with surface fluxes of latent and sensible heat that are vertically redistributed by moist convection. The lower boundary consists entirely of ocean with a specified SST given by the one-dimensional analog of (1),

$$T_s = T_0 + T_{\max}\frac{\pi}{2}\cos^2\left(\frac{\pi}{2}\frac{\phi - \phi_0}{\Delta\phi}\right), \tag{5}$$

with $\phi_0 = 25°$N and $\Delta\phi = 15°$, as in the dry model. This is used to specify the SST only between $\phi_0 - \Delta\phi$ and $\phi_0 + \Delta\phi$; outside this range T_s is set to T_0, with $T_0 = 296$ K. This provides an SST anomaly centered at 25°N and confined between 10° and 40°N, with no cross-equatorial SST gradient. The anomaly is prescribed to oscillate with the same seasonal cycle used for the dry model, given by (3).

Surface evaporation F_q is represented by a bulk formula:

$$F_q = \rho C_k |\mathbf{V}|[q^*(T_s) - q], \tag{6}$$

where ρ and q are the density and specific humidity of air at the lowest model level, C_k is a transfer coefficient set to 0.0012, and $q^*(\mathrm{T_s})$ is the saturation specific humidity at surface temperature T_s. Surface fluxes of sensible heat and momentum take a similar form, with the same nondimensional transfer coefficient. The effective wind speed is

$$|\mathbf{V}| = \sqrt{u^2 + v^2 + v_g^2}, \tag{7}$$

where u and v are the horizontal winds at the lowest model level. The parameter v_g is included to represent the effects of a range of subgrid-scale variations in wind, and in a more realistic treatment its value would vary with the local dynamic and thermodynamic state. Indeed, many surface flux formulas represent the effect of convective gustiness with a state-dependent velocity that typically has a value near 1 m s^{-1} for dry convection (Stull 1988) or up to about 5 m s^{-1} for precipitating convection (e.g., Williams 2001). For simplicity, we set v_g to the constant value of 4 m s^{-1}. This somewhat large value was chosen to suppress the formation of convective anomalies that propagate meridionally on intraseasonal time scales, which occur in this GCM for values of v_g less than about 3 m s^{-1}. Bellon and Sobel (2008) have examined what seem to be similar poleward-propagating anomalies in another axisymmetric model forced by steady SST, and proposed that they are relevant to the observed poleward migrations of the convective maximum associated with "active" and "break" episodes of the South Asian summer monsoon. The interaction of these propagating anomalies with the seasonal cycle may be relevant to the onset of monsoons, especially since the onset of the Indian monsoon is generally coincident with the first of several poleward migrations of a zonally elongated convective maximum during boreal summer (e.g., Yasunari 1979; Goswami 2005). These propagating anomalies are purposely suppressed here in order to focus first on the arguably simpler case of a classical, seasonally reversing Hadley circulation; we intend to examine the interaction of such anomalies with the seasonal cycle in future work.

Moist convection in this GCM is represented by the scheme of Emanuel and Zivkovic-Rothman (1999). Radiation is calculated by the longwave scheme of Morcrette (1991) and the shortwave scheme of Fouquart and Bonnel (1980). Insolation is independent of latitude and moves through a diurnal cycle, although the diurnal cycle has an effect only through atmospheric absorption of shortwave radiation because of the use of an entirely oceanic lower boundary with prescribed SST. Integrations are performed with no representation of cloud radiative effects (i.e., clear sky), and the specific humidity used for the radiative calculations is fixed at a reference profile that does not vary with latitude or time. Integrations with radiatively interactive specific humidity produced similar results, but with additional variability on time scales of 2–3 days that seemed extraneous to the physics of seasonal transitions. While the radiative effects of clouds are expected to alter the solutions, they are neglected here in order to better isolate the physics involving wind-dependent surface fluxes.

2) RUNS WITHOUT WISHE

We first discuss model integrations with $|\mathbf{V}|$ in the surface flux formulas for latent and sensible heat fixed at 5 m s^{-1}, thereby eliminating any effects of WISHE. The results are consistent with the findings of Zheng (1998), in that an AMC circulation occurs only when

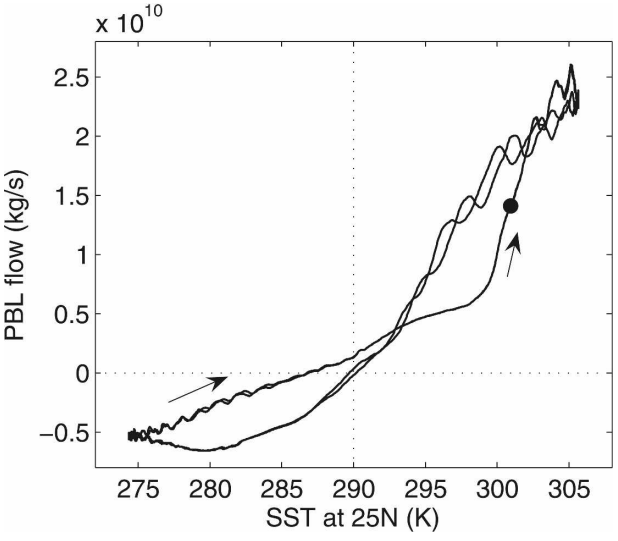

FIG. 6. As in Fig. 4, but the phase diagram for the moist GCM with strong forcing (θ_m = 10 K) and wind-independent surface enthalpy fluxes. The dot denotes the model state for which M and ψ are shown in Fig. 7.

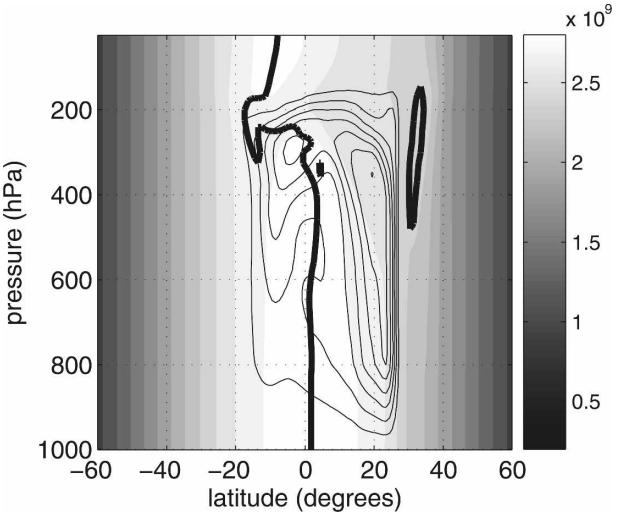

FIG. 7. As in Fig. 2 but for the moist GCM with strong forcing (θ_m = 10 K) and wind-independent surface enthalpy fluxes, at the time represented by the dot in Fig. 6. Streamfunction contour interval is 4×10^{10} kg s^{-1}, which is 4 times that used in Figs. 2 and 3.

the amplitude of the off-equatorial SST anomaly exceeds a certain threshold. For example, using θ_m = 10 K produces a phase-space trajectory resembling that obtained for the seasonally forced dry model with near-neutral stratification, in that the sensitivity of PBL flow to the amplitude of the SST anomaly increases abruptly as the anomaly nears its summer maximum (Fig. 6). Shortly after this increase in sensitivity (at a time indicated by the dot on the phase trajectory), M contours are strongly deformed from a resting state, with the zero contour of absolute vorticity η shifted to nearly 20°S near the tropopause (Fig. 7). The lower branch of the circulation crosses the equator well above the boundary layer, roughly following M contours in the free troposphere. This cross-equatorial jumping behavior presumably has such high amplitude because of interactions with moist convection, as discussed by Pauluis (2004).

When a much weaker forcing is used, with θ_m = 1 K and no WISHE, no abrupt intensification is seen (Fig. 8, gray line in left panel). This phase trajectory closely resembles the ellipse obtained for the seasonally forced dry model with an isothermal background state. The circulation near the time of peak SST is weak and confined entirely to the summer hemisphere, with M contours deviating only very slightly from the vertical in the upper troposphere (Fig. 9, right panel).

3) RUNS WITH WISHE

Now we examine a series of model integrations with surface enthalpy fluxes that depend on wind speed according to (6) and (7). As stated in the introduction, runs with WISHE will only be performed for forcings that are not strong enough to produce an AMC response. The effect of WISHE in an AMC regime is qualitatively different and will be explored in a separate paper.

For a run with WISHE and θ_m = 1 K, the circulation exhibits a rapid onset and withdrawal of the summer circulation, as indicated by the sudden increase in the slope of the phase trajectory near the time of maximum SST (Fig. 8, black line in left panel). Halfway through the abrupt intensification of the summer circulation in this WISHE run, M contours are slightly deformed from a resting state (Fig. 9, left panel), although they are far from the near-horizontal state in the upper troposphere characteristic of an AMC regime (cf. Fig. 7). The circulation at this time exists mostly in the summer hemisphere, consistent with a response that has not entered an AMC regime.

Given that the deformation of M contours is weak in the WISHE run, one might hypothesize that the abrupt intensification occurs because of a linear feedback between the strength of the Hadley circulation and the surface enthalpy flux. However, the abrupt onset of a strong solsticial circulation occurred only when both WISHE and nonlinear momentum advection were represented in the model. This was found by conducting a third model run with WISHE but without the advection of either zonal or meridional relative momentum. The phase trajectory of this run was nearly elliptical with a weak solsticial circulation and no abrupt transitions

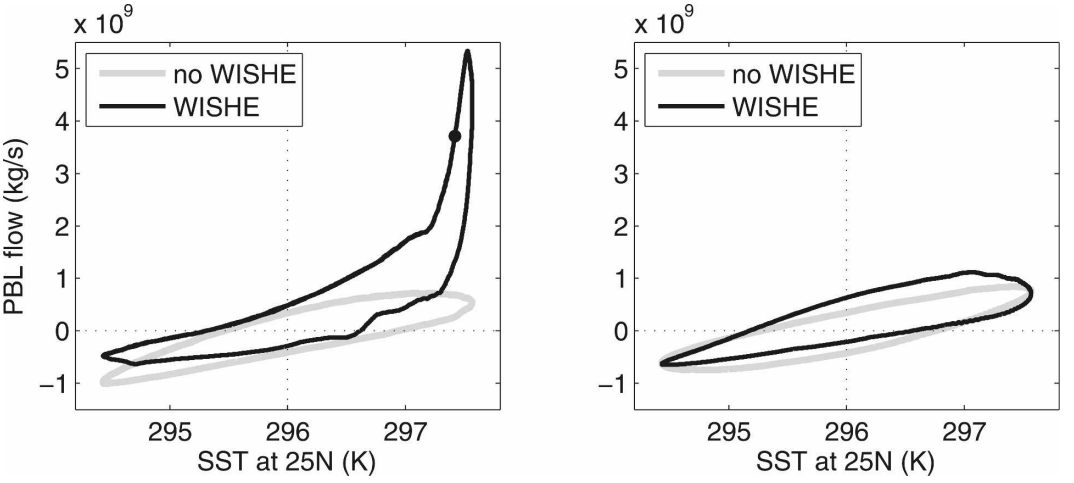

FIG. 8. As in Fig. 4, but the phase diagram for the moist GCM with weak forcing (θ_m = 1.0 K). Runs (left) with and (right) without nonlinear momentum advection are shown. The black and gray lines are for runs with and without WISHE, respectively. Dot in (left) denotes the time at which M and ψ are shown in Fig. 9.

(Fig. 8, right panel). Eliminating both WISHE and momentum advection in a fourth model run also produced a nearly elliptical phase trajectory. The use of WISHE without momentum advection did make the summer circulation almost twice as strong as the winter circulation, but this occurred without any rapid change in the slope of the phase trajectory and was a weak effect compared to that produced by the combination of WISHE and momentum advection.

Omitting the advection of relative momentum from the model equations without also omitting the advection of humidity and potential temperature results in nonconservation of total energy in the model. However, omitting all of these advection terms in an additional run produced a phase trajectory that differed only slightly from that of the run in which only relative momentum advection was omitted (not shown). This establishes that the combination of nonlinear advection and WISHE are both required for the abrupt intensification, and suggests that it is the nonlinear advection of momentum, in particular, that plays a central role in the feedback. An understanding of this interaction between WISHE and momentum advection will prove to be facilitated by use of an even simpler model, which is introduced in the next section.

3. Two-mode model

To better understand the nature of the abrupt intensification in the GCM run that employed both WISHE

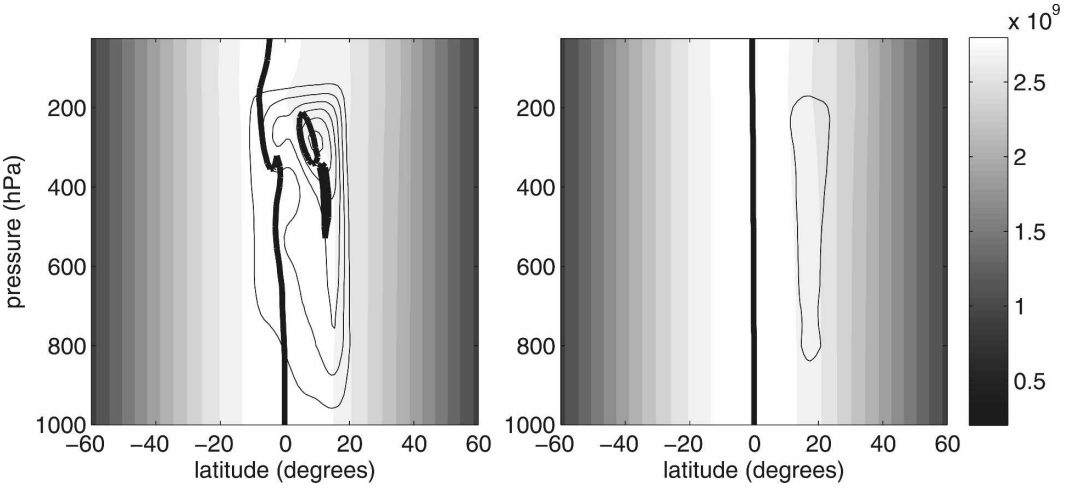

FIG. 9. As in Fig. 7, but for the moist GCM with weak forcing (θ_m = 1.0 K), at times denoted by the dot in Fig. 8. Runs (left) with and (right) without WISHE are shown (both included nonlinear momentum advection).

and nonlinear momentum advection, we implement a different axisymmetric model in which the assumption of convective quasi equilibrium is used to simplify the thermodynamics and in which only a barotropic mode and one baroclinic mode of the horizontal wind are represented.

a. Model formulation

1) General physics

This model is highly similar to the Quasi-Equilibrium Tropical Circulation Model (QTCM) of Neelin and Zeng (2000), but with the thermodynamics phrased in terms of moist entropy instead of temperature and humidity. This is done for consistency with previous theoretical studies of purely baroclinic WISHE modes by Emanuel (1987, 1993); an overview of the thermodynamics is given here, and the reader is directed to those papers for a more detailed derivation.

Moist convection is assumed to keep variations in s^*, the saturation moist entropy of the free troposphere, constant with height. This allows variations in the geopotential Φ to be partitioned into a barotropic component $\delta\Phi_0$ that is invariant with height, and a baroclinic component that can be written in terms of variations in s^*:

$$\frac{\partial}{\partial p}\delta\Phi = -\left(\frac{\partial T}{\partial p}\right)_{s^*}\delta s^* + \frac{\partial}{\partial p}\delta\Phi_0, \tag{8}$$

where the derivative of T is taken at constant s^*. In this particular model we assume no variations in surface pressure, so that the above can be integrated to obtain $\delta\Phi$:

$$\delta\Phi - \delta\Phi_b = (T_b - T)\delta s^*, \tag{9}$$

where the b subscript denotes a property at the top of the subcloud layer and T serves as a vertical coordinate. Using (9) together with the property that the vertical integral of purely baroclinic Φ perturbations must vanish gives

$$-\delta\Phi = (T - \overline{T})\delta s^*, \tag{10}$$

where $\overline{T}$ is a mass-weighted vertical mean tropospheric temperature.

Conservation equations, phrased on an equatorial β plane, for axisymmetric horizontal wind can then be written in terms of the fluctuating component of s^* (the δ symbol is henceforth omitted):

$$\frac{\partial u}{\partial t} + v\frac{\partial u}{\partial y} + w\frac{\partial u}{\partial z} - \beta y v = F_u$$

$$\frac{\partial v}{\partial t} + v\frac{\partial v}{\partial y} + w\frac{\partial v}{\partial z} + \beta y u = (T - \overline{T})\frac{\partial s^*}{\partial y} - \frac{\partial}{\partial y}\Phi_0 + F_v, \tag{11}$$

with the F terms representing both surface drag and diffusion.

Tendencies of s^* and subcloud-layer entropy s_b are

$$\frac{\partial s^*}{\partial t} + v\frac{\partial s^*}{\partial y} = -N^2(w - \epsilon M_c) - R + \kappa\frac{\partial^2 s^*}{\partial y^2}$$

$$H_b\left(\frac{\partial s_b}{\partial t} + v\frac{\partial s_b}{\partial y}\right) = E + \mathrm{MIN}[0, (w_b - M_c)](s_b - s_m) + H_b\kappa\frac{\partial^2 s_b}{\partial y^2}, \tag{12}$$

where M_c is the net upward mass flux in convective clouds, H_b is the depth of the subcloud layer, w_b is the vertical velocity at the top of the subcloud layer averaged over clear and cloudy areas, ϵ is a bulk precipitation efficiency, E is the surface entropy flux, and R is the rate of radiative cooling, which is fixed at 1 K day^{-1}. The second term on the right-hand side of the s_b equation represents the downward advection of low-entropy midtropospheric air into the boundary layer, with the difference between s_b and the midtropospheric entropy s_m hereafter assumed to be a constant, denoted χ. The MIN function is used to eliminate this term when the net mass flux is upward. Horizontal diffusion is represented with a constant diffusivity κ. A dry static stability is defined

$$N^2 \equiv c_p\Delta T\frac{\Gamma_d}{\Gamma_m}\frac{\partial \ln\theta}{\partial z}, \tag{13}$$

with Γ_d and Γ_m the dry and moist adiabatic temperature lapse rates, respectively. The surface entropy flux is given by a bulk transfer formula:

$$E = C_k|\mathbf{V}|(s_o^* - s_b), \tag{14}$$

where s_o^* is the saturation moist entropy at the temperature of the sea surface. Here $|\mathbf{V}|$ is given by (7) as for the primitive equation model, with the same surface gustiness of $v_g = 4$ m s^{-1}. For lower values of v_g, the model exhibits what seem to be meridionally propagating WISHE modes that are more intense than in the moist GCM. As discussed in the previous section, these transients may be relevant to actual monsoon circulations, and we hope to examine their interaction with the seasonal cycle in future work.

The subcloud-layer equilibrium is used to specify an equilibrium cloud-base mass flux:

$$M_{\mathrm{eq}} = w + \frac{1}{\chi}\left[E + H_b\left(\kappa\frac{\partial^2 s_b}{\partial y^2} - v\frac{\partial s_b}{\partial y}\right)\right]. \tag{15}$$

The actual convective mass flux is relaxed toward this equilibrium value over a time scale of 3 h, and is constrained to be nonnegative. We also set $M_c = 0$ if $s_b < s^*$, so that there is no convection where the atmosphere is stable.

2) Modal decomposition

The horizontal wind is projected onto a barotropic mode $\mathbf{v}_0$, and a baroclinic mode $\mathbf{v}_1$ that uses temperature as a vertical coordinate:

$$\mathbf{v} \equiv \mathbf{v}_0 + T'\mathbf{v}_1, \tag{16}$$

where T' is the temperature anomaly normalized by $\Delta T \equiv T_s - \overline{T}$:

$$T' \equiv \frac{T - \overline{T}}{\Delta T}. \tag{17}$$

The axisymmetric continuity equation

$$\frac{\partial w}{\partial z} + \frac{\partial v}{\partial y} = 0, \tag{18}$$

combined with the assumptions of no topography and constant surface pressure, gives a nondivergent barotropic wind. Under the constraint that v vanishes at the meridional boundaries, the barotropic wind must be purely zonal so that $v \equiv \mathrm{T}'v_1$. The horizontal wind is thus completely specified by u_0, u_1, and v_1, which depend on y and time only. No dynamical boundary layer is used in the momentum equations, and u_1 and v_1 can be taken to represent baroclinic winds at the surface.

With these assumptions, the vertical velocity must have a vertical structure independent of latitude and time:

$$w(y, z, t) \equiv \overline{w}(y, t)\Omega(z), \tag{19}$$

with the vertical structure obtained from the temperature profile,

$$\Omega(z) = \int_0^z T'\, dz. \tag{20}$$

In the axisymmetric two-mode framework, continuity is then

$$\overline{w} = -\frac{\partial v_1}{\partial y}. \tag{21}$$

Prognostic equations for u_1 and v_1 are obtained by substituting (16) into (11), multiplying by T', and integrating from the surface to the tropopause:

$$\begin{aligned}
&\frac{\partial u_1}{\partial t} + v_1\frac{\partial u_0}{\partial y} + \frac{\langle T'^3\rangle}{\langle T'^2\rangle}v_1\frac{\partial u_1}{\partial y} - \frac{\langle \Omega T'\partial_p T'\rangle}{\langle T'^2\rangle}\frac{\partial v_1}{\partial y}u_1 \\
&\qquad = \beta y v_1 - \frac{1}{\langle T'^2\rangle}\left[\frac{C_D}{H}|\mathbf{V}|(u_0 + u_1)\right] + \kappa\frac{\partial^2 u_1}{\partial y^2} \\
&\frac{\partial v_1}{\partial t} + \frac{\langle T'^3\rangle}{\langle T'^2\rangle}v_1\frac{\partial v_1}{\partial y} - \frac{\langle \Omega T'\partial_p T'\rangle}{\langle T'^2\rangle}\frac{\partial v_1}{\partial y}v_1 \\
&\qquad = \Delta T\frac{\partial s^*}{\partial y} - \beta y u_1 - \frac{1}{\langle T^2\rangle}\left[\frac{C_D}{H}|\mathbf{V}|v_1\right] + \kappa\frac{\partial^2 v_1}{\partial y^2},
\end{aligned} \tag{22}$$

where angle brackets represent mass-weighted vertical integrals, which are represented in pressure coordinates for simplicity. Quantities on the left-hand side are the time tendency and advective terms. Quantities on the right-hand side are the Coriolis, drag, and horizontal diffusion terms, with the v_1 equation also containing a pressure gradient forcing phrased in terms of s^*. Horizontal diffusion is used to represent some effects of eddies and to numerically stabilize the model. Vertical diffusion is neglected. The drag terms have been written using the same bulk flux formula for momentum as in the primitive equation model. The depth of the troposphere H is assumed constant.

A prognostic equation for the barotropic wind is calculated by integrating the zonal momentum equation in (11) in the vertical and taking the curl to give a barotropic vorticity equation:

$$\begin{aligned}
\frac{\partial \zeta_0}{\partial t} - \langle T'^2\rangle\frac{\partial^2}{\partial y^2}(v_1 u_1) &= \frac{\partial}{\partial y}\left[\frac{C_D}{H}|\mathbf{V}|(u_0 + u_1)\right] \\
&\quad + \kappa\frac{\partial^2 \zeta_0}{\partial y^2}.
\end{aligned} \tag{23}$$

The left-hand side contains the time tendency term and the advective terms written in flux form. The right-hand side contains the drag and horizontal diffusion terms, which use the same coefficients C_D and κ as for the baroclinic modes. The barotropic wind u_0 is obtained by inverting ζ_0.

The conservation equation for s^*, given in (12), must also be vertically integrated to eliminate the height dependence of w and M_c:

$$\frac{\partial s^*}{\partial t} = -N^2\langle\Omega\rangle(\overline{w} - \epsilon\overline{M}_c) - R + \kappa\frac{\partial^2 s^*}{\partial y^2}, \tag{24}$$

where R is assumed to be a prescribed, vertically uniform constant. This is the fully nonlinear conservation

TABLE 1. Parameters used in the two-mode model.

Parameter name	Symbol	Value
Surface minus mean atmospheric temperature	ΔT	35 K
Mean boundary layer depth	H_b	910 m
Mean tropopause height	H	14 km
Dry static stability	N^2	1.0 J kg^{-1} m^{-1}
Normalized second moment of temperature	$\langle T'^2 \rangle$	0.57
Normalized third moment of temperature	$\langle T'^3 \rangle$	−0.36
Correlation function for vertical advection	$\langle \Omega T' \partial_p T' \rangle$	−0.18
Vertical mean structure function	$\langle \Omega \rangle$	1.8×10^4
Structure function at top of subcloud layer	Ω_b	420 m
Mean subcloud-layer meridional wind	υ_b	0.89 υ_1
Horizontal diffusivity	κ	1.0×10^5 m^2 s^{-1}
Surface transfer coefficient for momentum	C_D	0.0012
Enthalpy exchange coefficient	C_k	0.0012
Surface gustiness	υ_g	4.0 m s^{-1}
Radiative cooling rate	R	1 K day^{-1}
Bulk precipitation efficiency	ϵ	0.85
Entropy drop at top of subcloud layer	$\theta_{eb} - \theta_m$	15 K
Gradient of Coriolis parameter	β	2.28×10^{-11} m^{-1} s^{-1}
Specific heat of air at constant pressure	c_p	1010 J kg^{-1} K^{-1}
Convective response time	τ_c	3 h

equation for s^*, where the horizontal advection term has been eliminated by the assumption that s^* is constant with height. The conservation equation for s_b does not need to be modified, although care must be taken to use the values of w and M_c at the top of the subcloud layer and the mean value of υ within that layer:

$$\left(H_b \frac{\partial s_b}{\partial t} + \upsilon_b \frac{\partial s_b}{\partial y} \right) = E + \mathrm{MIN}[0, (\overline{w} - \overline{M}_c)]\Omega_b \chi + H_b \kappa \frac{\partial^2 s_b}{\partial y^2}. \quad (25)$$

Here Ω_b is the value of Ω at the top of the subcloud layer, and υ_b is the mass-weighted meridional wind vertically averaged within the subcloud layer. The equilibrium mass flux then becomes

$$\overline{M}_{\mathrm{eq}} = \overline{w} + \frac{1}{\chi \Omega_b} \left[E + \left(H_b \kappa \frac{\partial^2 s_b}{\partial y^2} - \upsilon_1 \frac{\partial s_b}{\partial y} \Omega_b \right) \right], \quad (26)$$

with $\overline{M}_c$ relaxed toward $\overline{M}_{\mathrm{eq}}$ over a 6-h time scale.

The model consists of (13), (14), (17), and (21)–(26), which include the time tendency equations for the prognostic variables s^*, s_b, u_1, υ_1, and ζ_0. The parameters dependent on temperature were derived assuming a surface temperature of 296 K at 1000 hPa, a dry adiabat up to 900 hPa, and a moist pseudoadiabat from 900 to 150 hPa. The values used for model parameters are listed in Table 1. This model employs many simplifications even when compared to other reduced models of the tropical atmosphere, and because of this cannot represent a number of processes. In particular, it omits wave radiation into the stratosphere (Yano and Emanuel 1991), dynamical boundary layer effects (Sobel and Neelin 2006), moisture–radiation feedbacks, and some eddy transports. We do find, however, that it can represent the fundamental physics of the WISHE-induced abrupt seasonal transition seen in the moist GCM.

b. Linear properties

The above system includes nonlinear advection terms, which, because of the GCM results, we expect to be required for a WISHE feedback. It is of interest that Emanuel (1993) found purely baroclinic zonally symmetric circulations to be unstable to WISHE in a linearized version of the above system that employed no SST gradient and a basic state with easterly surface winds. While a basic state having a poleward SST gradient and westerly surface winds would be more relevant to the onset of the solsticial Hadley circulation, we discuss in the next section how the presence of a coupled barotropic circulation can stabilize WISHE modes in a linear system. Indeed, the Hadley circulation cannot be represented in terms of a purely baroclinic mode; a barotropic mode must be added to obtain zonal winds that are simultaneously strong at upper levels and weak at the surface, as discussed in detail by Burns et al. (2006). For this reason, a linear stability analysis of a purely baroclinic system is not presented here.

However, some insight can still be gained by exam-

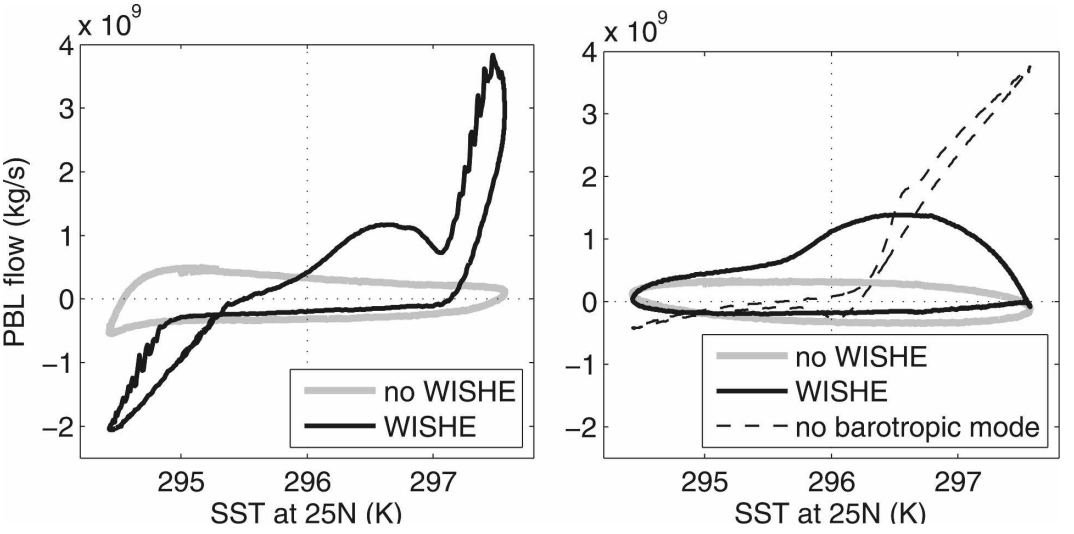

FIG. 10. As in Fig. 8 but for the two-mode model. (right) The dashed line is for a run with no barotropic wind and no nonlinear momentum advection, but with WISHE.

ining such a highly simplified, purely baroclinic system with dynamics linearized about a resting state. To do so, we neglect horizontal diffusion and represent surface drag as Rayleigh damping over a time scale $1/r$. For simplicity, we assume radiative cooling operates on the same time scale as this mechanical damping, so that R in (12) can be written as rs^*. We set the precipitation efficiency ϵ equal to unity, which corresponds to an atmosphere in which evaporatively driven downdrafts do not occur and free-tropospheric temperatures are controlled by boundary layer processes (Emanuel 1993). The system consisting of (11) and (12) can then be rewritten, assuming modal perturbations in u, v and s^* proportional to $e^{-i\omega t}$:

$$(r - i\omega)u = fv, \tag{27}$$

$$(r - i\omega)v = (T - \overline{T})\frac{\partial s^*}{\partial y} - fu, \quad \text{and} \tag{28}$$

$$(r - i\omega)s^* = \frac{N^2(T - \overline{T})}{\chi}E. \tag{29}$$

These can be combined into a single expression:

$$v = \left[\frac{1}{(r - i\omega)^2 + f^2}\right]\frac{N^2(T - \overline{T})}{\chi}\frac{\partial E}{\partial y}. \tag{30}$$

If the time scale of the damping is short compared to that of the forcing (i.e., $r \gg \omega$), then the real part of (30) is well approximated by

$$v \simeq \left(\frac{1}{r^2 + f^2}\right)\frac{N^2(T - \overline{T})}{\chi}\frac{\partial E}{\partial y}, \tag{31}$$

which is the same as the solution for the steady response to a time-invariant forcing. For ω corresponding to earth's seasonal cycle of insolation, this limit will hold if viscous losses are dominated by the strong vertical mixing of momentum in the planetary boundary layer, so that $1/r$ is on the order of a few days. This result then shows that the meridional gradient of the surface entropy flux is the relevant forcing for meridional flow, and that the flow will be nearly in phase with this forcing. If the circulation is instead controlled by nearly inviscid free-tropospheric dynamics, then such a linear treatment will likely not provide an appropriate description.

c. Numerical results

The fully nonlinear two-mode model is forced by the same time-varying SST used for the GCM, consisting of (3) and (5) with $\theta_m = 1$ K, and runs were performed with and without WISHE, and with and without nonlinear momentum advection. Although no explicit dynamical boundary layer exists in the two-mode model, the PBL flow was calculated by integrating meridional flow through the lowest 200 hPa of the atmosphere, to ease comparison with the GCM results. These phase-space trajectories are in many ways similar to those from the moist GCM, with an abrupt, high-amplitude intensification of the summer circulation occurring only when both WISHE and nonlinear momentum advection are used (Fig. 10). The two-mode model also exhibits an abrupt intensification of the winter circulation not seen in the GCM, although even in the two-mode model the winter circulation has about half the peak

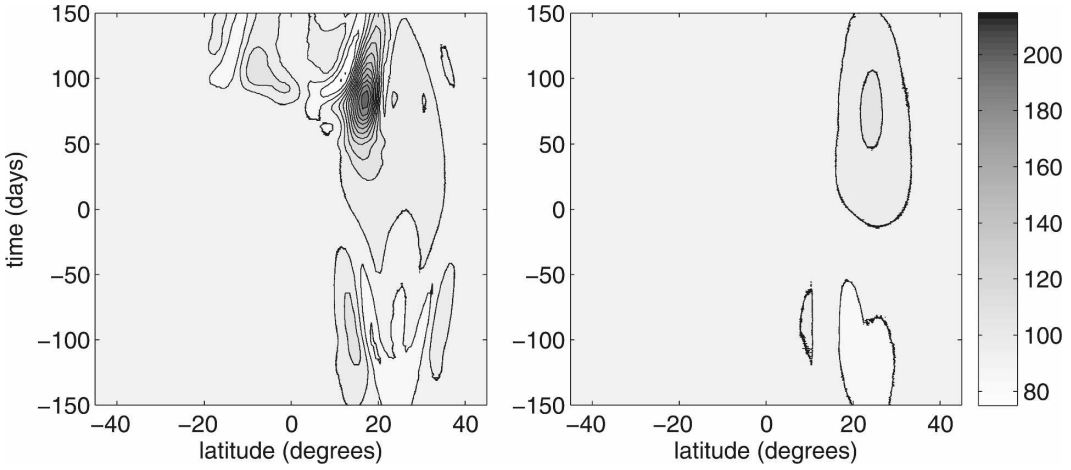

FIG. 11. Surface enthalpy flux for the moist GCM with weak forcing (θ_m = 1.0 K). Runs (left) with and (right) without WISHE are shown. Time is the number of days after SST has zero gradient, with maximum SST occurring at day 91 and 25°N. Contour interval is 10 W m^{-2}.

amplitude of the summer circulation. This abrupt intensification of the winter circulation can be eliminated (while preserving the abrupt summer intensification) by modifying several parameters of the two-mode model, in particular by using larger values of the surface gustiness, static stability, and horizontal diffusivity. The two-mode model in general seems more sensitive to the effects of WISHE, as even without momentum advection WISHE produces a fivefold increase in the peak PBL flow, although this increase occurs more slowly and is much weaker than that achieved in the model that includes both WISHE and momentum advection. Also, the phase-space trajectory for the run with both WISHE and momentum advection exhibits high-frequency oscillations about the mean trajectory during the rapid intensifications. While these oscillations are not associated with propagating instabilities, they might result from the same physics that would cause propagating WISHE modes at lower values of the surface gustiness parameter.

In the no-WISHE integrations of the two-mode model, the boundary layer flow peaked at least one-quarter cycle before the SST. This would seem to occur because of the relatively short phase lag between SST and subcloud-layer entropy. The surface entropy flux relaxes the entropy of the boundary layer toward that of the sea surface over the time scale τ_E:

$$\frac{E}{H_b} = \frac{1}{\tau_E}(s_o^* - s_b), \tag{32}$$

with $\tau_E \equiv H_b/(C_k|\mathbf{V}|)$. For typical values of these parameters, τ_E is on the order of 10 days, so that the phase lag between s_b and s_o^* is expected to be small compared to the 365-day period of s_o^*. Thus, the relation of E to the prescribed s_o^* is analogous to the relation of Newtonian cooling to the prescribed equilibrium temperature in the dry model. By the same trigonometric relationships used for the dry model to derive (4), E should then lead s_o^* by slightly less than one-quarter cycle, and the meridional circulation should be in phase with E. In such a simple linear theory, the major axis of the phase-space ellipse should be horizontal, as it nearly is for the two-mode model without WISHE. Although this contrasts with the GCM results where the major axis has a positive slope, such differences between the two-mode model and the GCM seem to result from phase lags in a predominantly linear response. Both models exhibit an abrupt intensification of solsticial flow due to the interaction of WISHE and nonlinear momentum advection.

4. Physics of the WISHE feedback

This section explains how the combination of WISHE and nonlinear momentum advection produces an abrupt intensification of the summer circulation in both the GCM and the two-mode model.

In the GCM run using both WISHE and nonlinear momentum advection, the surface enthalpy flux peaks about 8° south of the SST maximum, and this enthalpy flux peak is meridionally sharper than the SST peak (Fig. 11, left panel). Given that the meridional gradient of the surface enthalpy flux is the relevant forcing in a linear regime, it seems natural to ask how linear the atmospheric response is when viewed as a function of

this quantity.[2] We compute the mean value of $\partial_y E$ between 10°N and the latitude at which E peaks, and plot this quantity as a function of the SST at 25°N for the GCM runs with momentum advection and $\theta_m = 1$ K (Fig. 12). The resulting phase trajectories closely resemble the corresponding trajectories for meridional PBL flow in the moist GCM (cf. left panel of Fig. 8). Thus, the meridional circulation does not seem to be far from a linear response to $\partial_y E$, even though nonlinear dynamics are needed to achieve the positive feedback. This is an important point, because WISHE could be viewed simply as a way to reduce the critical SST gradient needed to obtain a nonlinear intensification from M advection, so that the same physics explored by PH92 and Zheng (1998) would apply at a lower SST threshold. The near-linear relationship between $\partial_y E$ and PBL flow is one piece of evidence that WISHE actually provides a separate mechanism for a nonlinear response of the PBL flow to the SST. Another piece of evidence is the small deformation of M contours in the runs with WISHE; the upper-tropospheric absolute vorticity is not uniformly zero over any nonvanishing region in either the GCM or the two-mode model for the forcing with $\theta_m = 1$ K (not shown).

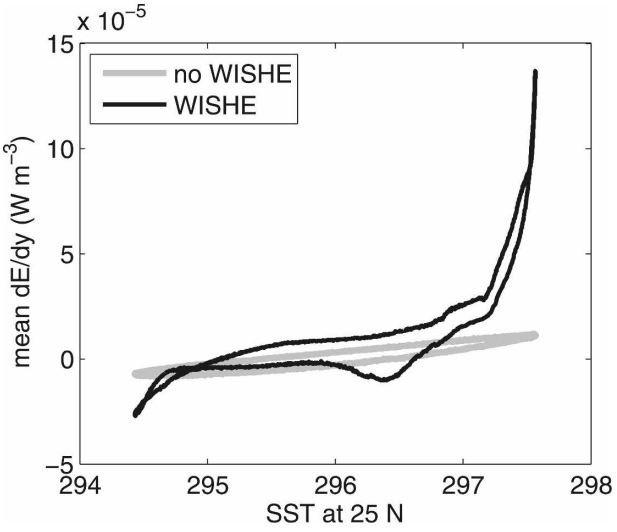

FIG. 12. Phase diagram, for the moist GCM with weak forcing ($\theta_m = 1.0$ K), of the meridional mean meridional gradient of surface enthalpy fluxes, with the mean taken between the enthalpy flux peak and 10°N, plotted against the SST at 25°N. The black and gray lines are for runs with and without WISHE, respectively, both with nonlinear momentum advection.

If the net meridional mass flux exhibits a near-linear response to the surface enthalpy flux, why does WISHE not produce an abrupt onset when momentum advection is omitted from the model? The reason for this was briefly mentioned above in discussion of the linear properties of the two-mode model. Emanuel (1993) showed that zonally symmetric, purely baroclinic circulations can be linearly unstable to WISHE. The Hadley circulation, however, projects strongly onto a barotropic mode, with surface winds that are generally weak compared to upper-tropospheric winds. Since WISHE instabilities arise from enthalpy flux anomalies driven by surface winds, a reduction in the magnitude of surface winds by the partial cancellation of the baroclinic and barotropic components of zonal wind at the surface would be expected to reduce or even eliminate any instability. This hypothesis was tested by eliminating the barotropic mode from a version of the two-mode model linearized about a resting state. The resulting circulation exhibited an abrupt increase in its sensitivity to SST as soon as the SST gradient changed sign to become positive in the tropics (Fig. 10, right panel). While such a change in sensitivity should not necessarily be interpreted as an instability, WISHE clearly has a stronger effect on circulations with linear dynamics in the absence of a coupled barotropic mode. When WISHE was turned off with the barotropic mode eliminated, the phase trajectory was nearly elliptical with a much weaker meridional flow (not shown).

In the two-mode model without WISHE but with momentum advection, the barotropic zonal wind does, in general, nearly cancel the low-level baroclinic wind everywhere (Fig. 13, right column). In the upper troposphere, the two modes must then add to produce strong easterlies south of the SST maximum during "summer" conditions. In the two-mode model with both WISHE and momentum advection, the barotropic wind opposes the surface baroclinic wind nearly everywhere except just south of the SST extremum during solstice conditions, during the time when the rapid intensification of PBL flow occurs (Fig. 13, left column). During summer, the two modes add to produce a narrow region of strong surface westerlies, which are in turn associated with strong surface enthalpy fluxes. The conservation equation for barotropic zonal wind (23) shows that in a region of baroclinic surface westerlies, the only process that can make the barotropic wind more westerly is convergence of the meridional flux of zonal momentum. A similar though somewhat weaker effect is seen during winter, when barotropic and baroclinic easterlies add to produce a narrow band of strong surface easterlies near 12°N.

Similar dynamics seem to occur in the moist GCM, although the low-level constructive superposition of

[2] At the SSTs used here, the enthalpy flux is very close to a constant linear multiple of the entropy flux, so we use the two somewhat interchangeably in this section.

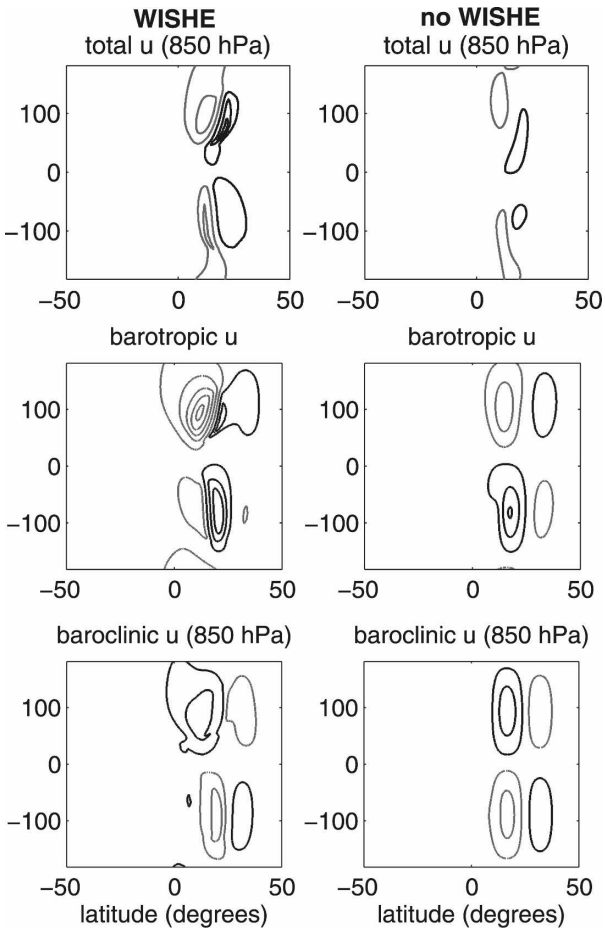

FIG. 13. Decomposition of the low-level zonal wind in the two-mode model. Runs (left column) with and (right column) without WISHE are shown. Both of these runs included nonlinear momentum advection. (top row) The total zonal wind at 850 hPa, (middle row) the barotropic component, and (bottom row) the baroclinic component at 850 hPa are shown. Black lines denote westerlies and gray lines easterlies, with a contour interval of 5 m s^{-1} starting at 2.5 m s^{-1}. Time is the number of days after the SST has zero gradient, with maximum SST occurring at day 91 and 25°N.

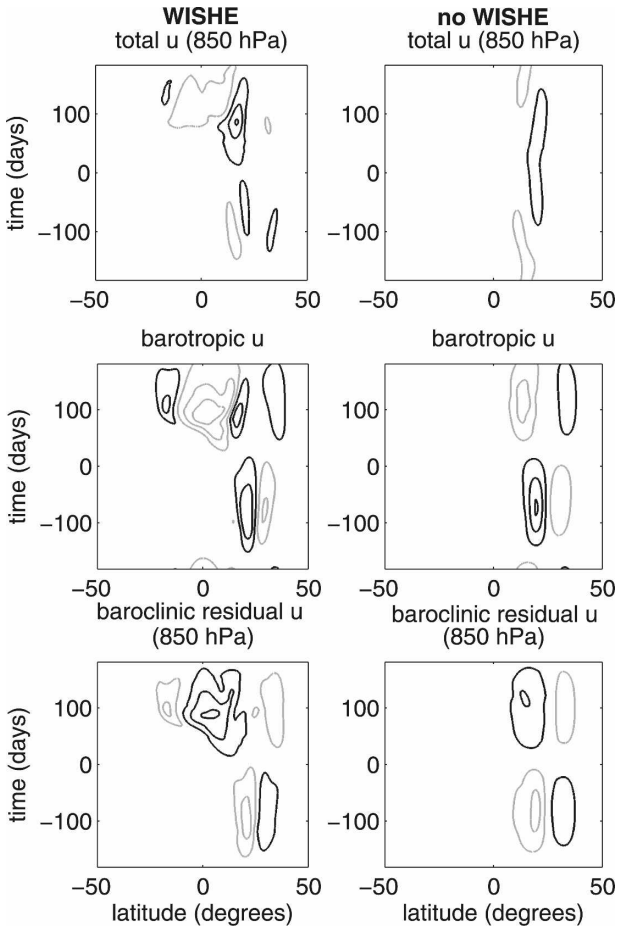

FIG. 14. As in Fig. 13, but for the moist GCM with weak forcing (θ_m = 1.0 K). The barotropic component is a vertical tropospheric mean, and the baroclinic residual was obtained by subtracting this barotropic component from the total zonal wind.

barotropic and baroclinic modes occurs only during summer. A barotropic wind was defined as the mass-weighted vertical mean zonal wind between the surface and the tropopause, with the tropopause defined as the level at which the static stability increased sharply to stratospheric values. Instead of a particular baroclinic mode, we examine the residual obtained by subtracting the barotropic wind from the total zonal wind. In the run conducted without WISHE but with momentum advection, the barotropic zonal wind and this baroclinic residual nearly cancel at low levels (Fig. 14, right column). In the run with both WISHE and momentum advection, the meridional structure of these modes is similar to that seen in the two-mode model: the barotropic wind adds to the low-level baroclinic residual only near the ascent branch of the circulation just south of the SST maximum (Fig. 14, left column).

In both the two-mode model and the GCM, then, a positive feedback seems to occur when the convergence of the meridional flux of zonal momentum becomes sufficiently strong to produce a barotropic wind that adds to the surface baroclinic wind instead of opposing it, thereby eliminating the damping effect of the barotropic mode on the wind–evaporation feedback. The mean meridional circulation will, in a vertical mean, converge zonal momentum into the ascending branch as long as M contours tilt toward the equator with height. Because such a tilt is brought about by advection in a model that conserves M, convergence of zonal momentum into the ascending branch will be accomplished by any mean meridional flow as long as this flow is directed poleward at low levels, a fairly general condition for any thermally direct, solsticial flow. To

create barotropic westerlies, this momentum convergence must overcome surface drag and any other horizontal transports:

$$-\left\langle \frac{\partial(vu)}{\partial y} \right\rangle > -\frac{C_D}{H}|\mathbf{V}|u + F. \tag{33}$$

Here H is the depth of the troposphere and F represents horizontal transports including diffusion and momentum transports by zonally asymmetric eddies (which do not occur in the models examined in this paper).

In the simplified case where F is zero and surface drag is a linear Rayleigh damping, a scale estimate of the terms in (33) provides

$$\frac{V}{\Delta y} > r, \tag{34}$$

where V is the velocity scale of the meridional wind, r is the damping coefficient, and Δy is the meridional scale over which the circulation changes. If V responds linearly to the forcing, as in (31), then this amounts to a condition on the curvature of the surface entropy flux.

While this scaling is likely too crude to be quantitatively compared with the numerical model results, it does show that a critical surface entropy flux gradient should exist below which no wind–evaporation feedback will occur. We test for the existence of such a threshold by changing the peak amplitude of the SST forcing in the two-mode model (integrated with both WISHE and nonlinear momentum advection). The case examined thus far with $\theta_m = 1$ K seems to nearly coincide with this threshold. A run using $\theta_m = 0.5$ K had no abrupt intensification, and a run using $\theta_m = 1.5$ K had an abrupt intensification reaching a much higher amplitude (Fig. 15). The run with $\theta_m = 1.5$ K exhibited high-amplitude transient instabilities, of somewhat different form than those found by Bellon and Sobel (2008), and their effect on the phase trajectory was reduced by applying a 10-day moving average. Although this smoothing also reduced the apparent abruptness of the onset of summer flow in the resulting phase trajectory, it is interesting that the smoothed trajectory has a similar shape to that seen for weaker forcings which do not produce transient instabilities. That is, it might be possible to use the mechanisms described in this paper to describe a smoothed version of the seasonal dynamics even when such instabilities occur, a hypothesis that may merit further examination in future work. Note that the forcing with $\theta_m = 1.5$ K did not produce an AMC response, as indicated by nonzero values of upper-tropospheric absolute vorticity in this model throughout its seasonal cycle (not shown).

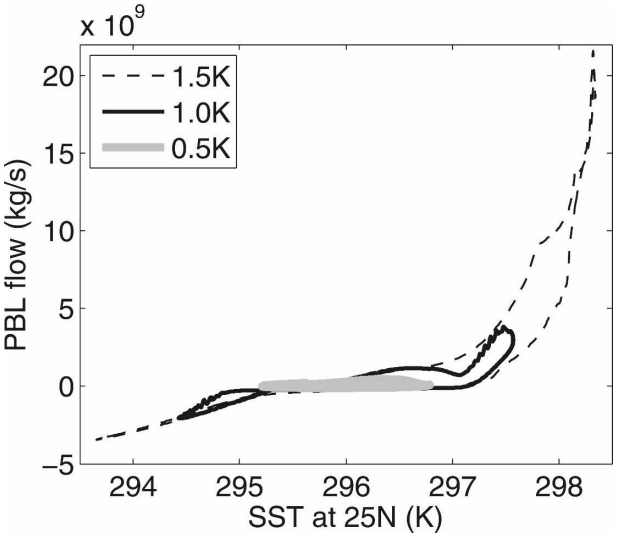

FIG. 15. As in Fig. 8 but for the two-mode model with SST forcings of different strengths. All runs included both WISHE and nonlinear momentum advection. Dashed line is for $\theta_m = 1.5$ K, solid black line for 1.0 K, and solid gray line for 0.5 K. The solid black line is the same trajectory appearing in (left) of Fig. 10.

5. Concluding remarks

A seasonal cycle that is long compared to the time scale of meridional M advection should be a necessary, albeit not sufficient, condition for the scalings and thresholds of nonlinear axisymmetric theories (e.g., Held and Hou 1980; PH92) to apply to an arbitrary planetary atmosphere. We have found that the dry axisymmetric models used by some previous studies (e.g., Fang and Tung 1999) equilibrate too slowly to be used for study of the time-dependent response to earth's seasonal insolation forcing, but that moist axisymmetric models equilibrate much faster because of their characteristic stratification and radiative cooling rate. This makes examination of the seasonal cycle in a moist atmosphere, which when fully represented will include effects of WISHE, a logical extension of previous work on nonlinear axisymmetric flow.

This paper focused on fairly weak SST forcings that did not produce an AMC response. In the axisymmetric models used here, WISHE produced meridional flow that increased nonlinearly as a function of the seasonally evolving SST gradient, even though the flow never transitioned into an AMC regime. For Hadley circulations with a strong barotropic component, this WISHE

feedback was found to occur only when the vertically integrated convergence of zonal momentum into the ascent branch of the circulation was larger than the momentum sink due to surface drag and any other horizontal transports. The effect of WISHE for stronger SST forcings that do produce an AMC response will be examined in a separate paper. Examination of SST forcings with nonzero gradients on the equator is also left for this separate work, as such forcings are expected to produce AMC flow regardless of their amplitude (as discussed in PH92).

Numerous physical processes omitted from the models used here may affect the physics of the WISHE feedback. Using an SST anomaly as a proxy for the thermal forcing of a land surface allows WISHE to operate over the entire domain, whereas the relatively small thermal inertia of a land surface should eliminate WISHE for periods longer than 5–10 days (e.g., Neelin et al. 1987; Maloney and Sobel 2004). How the WISHE feedback might alter monsoon onset when it operates only over the ocean equatorward of a coast could be easily explored in a variation on the axisymmetric models used here. Of course, the effect of a land surface may extend beyond that of its surface enthalpy flux, as elevated topography in the South Asian monsoon is known to strongly organize the flow (e.g., Hoskins and Rodwell 1995) and to increase free-tropospheric temperatures (e.g., Molnar and Emanuel 1999).

The radiative effects of variable clouds and water vapor were also omitted from our models. Ackerman and Cox (1987) estimated horizontal variations in atmospheric radiative flux divergence of about 100 W m^{-2} between clear and cloudy oceanic regions in the 1979 Asian summer monsoon, which is similar to the magnitude of wind-induced surface enthalpy flux variations in our models. Bony and Emanuel (2005) found that moisture–radiation feedbacks can have a scale-selecting effect on WISHE modes and also excite additional small-scale instabilities. Both of these results suggest that the role of moisture–radiation feedbacks in monsoon onset merit further study.

SST in our models was treated as a prescribed forcing, and it is known that surface winds alter SST by driving ocean evaporation, dynamical transports, and the entrainment of thermocline water into the ocean mixed layer. While a common practice in idealized models is to treat the ocean as a dynamically passive bulk mixed layer, and use of such a mixed layer would be a useful extension of this work, it is not obvious that these processes are more important than dynamical ocean transports in monsoon regions. Indeed, Webster and Fasullo (2003) proposed that the seasonally reversing, cross-equatorial heat flux in the Indian Ocean regulates the strength of the South Asian monsoon. While they focused on interannual variability, dynamical ocean transports might play a role in modulating any abrupt seasonal transitions.

We noted in the introduction that eddy momentum transports may play a role in monsoon onset. Eddy transports might even play a direct role in the WISHE feedback because this feedback requires the convergence of zonal momentum to overcome the damping effects of the barotropic wind. However, in the dry model used by Schneider and Bordoni (2008), the ascending branch of the cross-equatorial cell was associated almost entirely with momentum transports by the mean meridional circulation, with eddies extracting zonal momentum primarily from the subsiding branch of the Hadley circulation and depositing it in higher latitudes of the winter hemisphere. There would thus be no a priori reason to believe that eddy momentum transports would oppose the momentum convergence required for the WISHE feedback.

Finally, the physics of WISHE may change profoundly with both the structure of the forcing and the breaking of axisymmetry. Prive and Plumb (2007) illustrated the large effect zonal asymmetries in a forcing can have on the atmospheric response. Yet even with a zonally symmetric forcing, Emanuel (1993) showed that growth rates for WISHE modes peak at a nonzero zonal wavenumber, which suggests that WISHE feedbacks in three dimensions might possess a different sensitivity to SST gradients than in axisymmetric models. Thus, to apply the ideas in this paper to actual monsoon circulations, it will eventually be necessary to understand the behavior of WISHE modes in a three-dimensional domain with ocean, land, and radiative interactions.

Acknowledgments. This research constituted part of the first author's doctoral thesis, and was supported by the National Science Foundation under Grant ATM-0432090. We thank Arnaud Czaja and Nikki Privé for assistance with the GCM, which was originally implemented by Olivier Pauluis and Sandrine Bony. Discussions with Alan Plumb, Tapio Schneider, and Masahiro Sugiyama were valuable in the preparation of this work. Comments by Adam Sobel and an anonymous reviewer greatly improved the presentation and content of this paper.

APPENDIX

Equilibration Time Scale of Axisymmetric Models

The nonlinear dependence of circulation strength on the forcing in axisymmetric theory results from advec-

TABLE A1. Estimated equilibration time scales.

Model	Temperature profile	Stratification (S)	Heating rate (Q)	τ_M
Plumb and Hou (1992)	Isothermal	-2×10^{-3} K Pa^{-1}	0.5 K day^{-1}	165 days
Fang and Tung (1999)	$\Gamma = 6$ K km^{-1}	-5×10^{-4} K Pa^{-1}	0.3 K day^{-1}	75 days
Zheng (1998)/Moist GCM	Moist adiabat	-5×10^{-4} K Pa^{-1}	1 K day^{-1}	25 days
Near-neutral stratification	$\Gamma = 0.9\, g/c_p$	-2×10^{-4} K Pa^{-1}	0.5 K day^{-1}	15 days

tion of absolute angular momentum in the free troposphere, so the relevance of this nonlinearity in a time-dependent scenario would seem to depend on the magnitude of the momentum advection time scale relative to the forcing time scale. PH92 found that it took as long as 400 days for their dry axisymmetric model to reach a steady state, and suggested that this resulted from the roughly 100-day time scales for viscous dissipation and meridional overturning in their model. Presumably, the equilibration rate would be set by the overturning time scale in the inviscid limit, so here we use a simple scaling argument to explicitly estimate the time scale for angular momentum advection in axisymmetric models.

The circulation in the interior of an inviscid atmosphere will conserve absolute angular momentum M:

$$M = \Omega_e a^2 \cos^2\phi + ua\cos\phi, \tag{A1}$$

where Ω_e is the planetary rotation rate, a is the planetary radius, u is zonal velocity, and ϕ is latitude. In an atmosphere near a resting state, advection will be almost entirely meridional until M surfaces deviate considerably from the vertical. A scale estimate for the meridional wind v can be obtained from the thermodynamic equation under the assumption that the dominant balance is between the diabatic heating Q and vertical advection of potential temperature θ:

$$\omega S \sim \frac{Q}{c_p}, \tag{A2}$$

where ω is vertical velocity in pressure coordinates, $S \equiv \partial_p \theta$, and c_p is the specific heat at constant pressure. The meridional circulation will adjust quite rapidly to satisfy (A2): Eliassen (1951) showed that the thermally forced meridional circulation in an axisymmetric vortex equilibrates on a time scale near that of the local inertial period. The bulk of the free-tropospheric meridional flow will occur over some vertical distance Δp and some horizontal distance $\Delta y = y_2 - y_1$ (we use Cartesian coordinates for simplicity). By continuity in a zonally symmetric fluid,

$$v = -\int_{y_1}^{y_2} \frac{\partial \omega}{\partial p}\, dy \sim \frac{Q\Delta y}{Sc_p\Delta p}. \tag{A3}$$

The time scale τ_M for meridional advection is then

$$\tau_M \sim \frac{Sc_p\Delta p}{Q}. \tag{A4}$$

Although Δp and Q are part of the solution, approximate values can be estimated based on previous model results. For example, a value of half the tropospheric depth seems reasonable for Δp, unless flow becomes concentrated in a boundary layer. Similarly, Q is constrained by the equilibrium temperature and relaxation time imposed by the Newtonian cooling scheme in a dry model, or by radiation in a moist model.

Estimates of τ_M for several models are presented in Table A1. The fact that the integrations conducted by Plumb and Hou (1992) took hundreds of days to equilibrate is consistent with the parameters of their model: $\Delta p = 400$ hPa and values of S and Q appropriate for relaxation over a 10-day time scale to a temperature profile that was isothermal in the vertical and had maximum horizontal anomalies of about 10 K. The dry model of Fang and Tung (1999) used a stratification characteristic of a moist adiabat, but prescribed temperature relaxation over a 20-day time scale to produce typical Newtonian cooling rates of 0.3 K day^{-1} (inferred from their figures). It should be noted that τ_M is the time scale for M advection, and that the M field will likely take several times this long to fully equilibrate. Thus, although τ_M for the Fang and Tung (1999) model is only slightly larger than the time scale of their applied thermal forcing (365 days/2π = 58 days), the M field in their model cannot be expected to achieve equilibrium when subjected to such a forcing.

In contrast, a value of $\tau_M = 25$ days is obtained if one uses the same value of Δp but with a stratification typical of a moist adiabat and a radiative cooling rate of 1 K day^{-1}, typical values for the tropical troposphere. Such an average radiative cooling rate is the appropriate value for Q if the intensity of meridional flow is required to be consistent with a balance between radiative cooling and adiabatic heating in the subsiding branch of the circulation (e.g., Nilsson and Emanuel 1999; Emanuel et al. 1994). The value of τ_M may be reduced below the value given in Table A1 because free-tropospheric Hadley flow typically occurs within

about 200 hPa of the tropopause (Peixoto and Oort 1992). In any case, the time scale of earth's insolation forcing is at least 2–3 times greater than τ_M for parameters relevant to a moist tropical atmosphere, which explains why Zheng (1998) achieved large M deformation on seasonal time scales in his moist model.

REFERENCES

Ackerman, S. A., and S. K. Cox, 1987: Radiative energy budget estimates for the 1979 southwest summer monsoon. *J. Atmos. Sci.,* **44,** 3052–3078.

Adcroft, A. J., C. N. Hill, and J. C. Marshall, 1999: A new treatment of the Coriolis terms in C-grid models at both high and low resolutions. *Mon. Wea. Rev.,* **127,** 1928–1936.

Bellon, G., and A. H. Sobel, 2008: Poleward-propagating intraseasonal monsoon disturbances in an intermediate-complexity axisymmetric model. *J. Atmos. Sci.,* **65,** 470–489.

Bony, S., and K. A. Emanuel, 2005: On the role of moist processes in tropical intraseasonal variability: Cloud–radiation and moisture–convection feedbacks. *J. Atmos. Sci.,* **62,** 2770–2789.

Burns, S., A. Sobel, and L. Polvani, 2006: Asymptotic solutions of the axisymmetric moist Hadley circulation in a model with two vertical modes. *Theor. Comput. Fluid Dyn.,* **20,** 443–467.

Dima, I. M., and J. M. Wallace, 2003: On the seasonality of the Hadley cell. *J. Atmos. Sci.,* **60,** 1522–1527.

Dunkerton, T. J., 1989: Nonlinear Hadley circulation driven by asymmetric differential heating. *J. Atmos. Sci.,* **46,** 956–974.

Eliassen, A., 1951: Slow thermally or frictionally controlled meridional circulation in a circular vortex. *Astrophys. Norv.,* **5,** 19–60.

Emanuel, K. A., 1987: Air–sea interaction model of intraseasonal oscillations in the tropics. *J. Atmos. Sci.,* **44,** 2324–2340.

——, 1993: The effect of convective response time on WISHE modes. *J. Atmos. Sci.,* **50,** 1763–1775.

——, and M. Zivkovic-Rothman, 1999: Development and evaluation of a convection scheme for use in climate models. *J. Atmos. Sci.,* **56,** 1766–1782.

——, J. D. Neelin, and C. S. Bretherton, 1994: On large-scale circulations in convecting atmospheres. *Quart. J. Roy. Meteor. Soc.,* **120,** 1111–1143.

Fang, M., and K. K. Tung, 1999: Time-dependent nonlinear Hadley circulation. *J. Atmos. Sci.,* **56,** 1797–1807.

Findlater, J., 1969: A major low-level air current near the Indian Ocean during the northern summer. *Quart. J. Roy. Meteor. Soc.,* **95,** 362–380.

Fouquart, Y., and B. Bonnel, 1980: Computation of solar heating of the Earth's atmosphere: A new parameterization. *Beitr. Phys. Atmos.,* **53,** 35–62.

Goswami, B. N., 2005: South Asian summer monsoon. *Intraseasonal Variability in the Atmosphere-Ocean Climate System,* W. Lau and D. Waliser, Eds., Springer Praxis, 125–173.

Halpern, D., and P. M. Woiceshyn, 1999: Onset of the Somali Jet in the Arabian Sea during June 1997. *J. Geophys. Res.,* **104** (C8), 18 041–18 046.

Held, I. M., and A. Y. Hou, 1980: Nonlinear axially symmetric circulations in a nearly inviscid atmosphere. *J. Atmos. Sci.,* **37,** 515–533.

Hoskins, B. J., and M. J. Rodwell, 1995: A model of the Asian summer monsoon. Part I: The global scale. *J. Atmos. Sci.,* **52,** 1329–1340.

Krishnamurti, T. N., P. Ardanuy, Y. Ramanathan, and R. Pasch, 1981: On the onset vortex of the summer monsoon. *Mon. Wea. Rev.,* **109,** 344–363.

Lindzen, R. S., and A. Y. Hou, 1988: Hadley circulation for zonally averaged heating centered off the Equator. *J. Atmos. Sci.,* **45,** 2416–2427.

Maloney, E., and A. Sobel, 2004: Surface fluxes and ocean coupling in the tropical intraseasonal oscillation. *J. Climate,* **17,** 4368–4386.

Mapes, B., P. Liu, and N. Buenning, 2005: Indian monsoon onset and the Americas midsummer drought: Out-of-equilibrium responses to smooth seasonal forcing. *J. Climate,* **18,** 1109–1115.

Marshall, J., A. Adcroft, C. Hill, L. Perelman, and C. Heisey, 1997: A finite-volume, incompressible Navier Stokes model for studies of the ocean on parallel computers. *J. Geophys. Res.,* **102** (C3), 5753–5766.

——, ——, J.-M. Campin, and C. Hill, 2004: Atmosphere–ocean modeling exploiting fluid isomorphisms. *Mon. Wea. Rev.,* **132,** 2882–2894.

Molnar, P., and K. A. Emanuel, 1999: Temperature profiles in radiative-convective equilibrium above surfaces at different heights. *J. Geophys. Res.,* **104,** 24 265–24 272.

Morcrette, J.-J., 1991: Radiation and cloud radiative properties in the European Centre for Medium-Range Weather Forecasts forecasting system. *J. Geophys. Res.,* **96,** 9121–9132.

Murakami, T., L.-X. Chen, and A. Xie, 1986: Relationship among seasonal cycles, low-frequency oscillations, and transient disturbances as revealed from outgoing long-wave radiation data. *Mon. Wea. Rev.,* **114,** 1456–1465.

Neelin, J. D., and N. Zeng, 2000: A quasi-equilibrium tropical circulation model: Formulation. *J. Atmos. Sci.,* **57,** 1741–1766.

——, I. M. Held, and K. H. Cook, 1987: Evaporation-wind feedback and low-frequency variability in the tropical atmosphere. *J. Atmos. Sci.,* **44,** 2341–2348.

Nilsson, J., and K. A. Emanuel, 1999: Equilibrium atmospheres of a two-column radiative-convective model. *Quart. J. Roy. Meteor. Soc.,* **125,** 2239–2264.

Numaguti, A., 1995: Dynamics and energy balance of the Hadley circulation and the tropical precipitation zones. Part II: Sensitivity to meridional SST distribution. *J. Atmos. Sci.,* **52,** 1128–1141.

Pauluis, O., 2004: Boundary layer dynamics and cross-equatorial Hadley circulation. *J. Atmos. Sci.,* **61,** 1161–1173.

——, and K. Emanuel, 2004: Numerical instability resulting from infrequent calculation of radiative heating. *Mon. Wea. Rev.,* **132,** 673–686.

Peixoto, J. P., and A. H. Oort, 1992: *Physics of Climate.* American Institute of Physics, 520 pp.

Plumb, R. A., and A. Y. Hou, 1992: The response of a zonally symmetric atmosphere to subtropical thermal forcing: Threshold behavior. *J. Atmos. Sci.,* **49,** 1790–1799.

Prive, N. C., and R. A. Plumb, 2007: Monsoon dynamics with interactive forcing. Part II: Impact of eddies and asymmetric geometries. *J. Atmos. Sci.,* **64,** 1431–1442.

Rotunno, R., 1983: On the linear theory of the land and sea breeze. *J. Atmos. Sci.,* **40,** 1999–2009.

Schneider, E. K., 1977: Axially symmetric steady-state models of the basic state for instability and climate studies. Part II. Nonlinear calculations. *J. Atmos. Sci.,* **34,** 280–296.

Schneider, T., and S. Bordoni, 2008: Eddy-mediated regime transitions in the seasonal cycle of a Hadley circulation and implications for monsoon dynamics. *J. Atmos. Sci.,* **65,** 915–934.

Sobel, A., and J. Neelin, 2006: The boundary layer contribution to

intertropical convergence zones in the quasi-equilibrium tropical circulation model framework. *Theor. Comput. Fluid Dyn.,* **20,** 323–350.

Stull, R. B., 1988: *An Introduction to Boundary Layer Meteorology.* Kluwer Academic, 666 pp.

Walker, C. C., and T. Schneider, 2005: Response of idealized Hadley circulations to seasonally varying heating. *Geophys. Res. Lett.,* **32,** L06813, doi:10.1029/2004GL022304.

——, and ——, 2006: Eddy influences on Hadley circulations: Simulations with an idealized GCM. *J. Atmos. Sci.,* **63,** 3333–3350.

Webster, P. J., and J. Fasullo, 2003: Monsoon: Dynamical theory. *Encyclopedia of Atmospheric Sciences,* J. R. Holton, J. A. Curry, and J. A. Pyle, Eds., Academic Press, 1370–1385.

——, V. O. Magana, T. N. Palmer, J. Shukla, R. A. Tomas, M. Yanai, and T. Yasunari, 1998: Monsoons: Processes, predictability, and the prospects for prediction. *J. Geophys. Res.,* **103** (C7), 14 451–14 510.

Wheeler, M. C., and J. L. McBride, 2005: Australian-Indonesian monsoon. *Intraseasonal Variability in the Atmosphere-Ocean Climate System,* W. Lau and D. Waliser, Eds., Springer Praxis, 125–173.

Williams, A. G., 2001: A physically based parametrization for surface flux enhancement by gustiness effects in dry and precipitating convection. *Quart. J. Roy. Meteor. Soc.,* **127,** 469–491.

Yano, J.-I., and K. Emanuel, 1991: An improved model of the equatorial troposphere and its coupling with the stratosphere. *J. Atmos. Sci.,* **48,** 377–389.

Yasunari, T., 1979: Cloudiness fluctuation associated with the northern hemisphere summer monsoon. *J. Meteor. Soc. Japan,* **57,** 227–242.

Zheng, X., 1998: The response of a moist zonally symmetric atmosphere to subtropical surface temperature perturbation. *Quart. J. Roy. Meteor. Soc.,* **124,** 1209–1226.